Electrospray Mass Spectrometric Detection of Products and Short-Lived Intermediates in Aqueous Aerosol Microdroplets Exposed to a Reactive Gas

S. Enami, C. D. Vecitis, J. Cheng, M. R. Hoffmann, and A. J. Colussi*

W. M. Keck Laboratories, California Institute of Technology, Pasadena, California 91125

Received: July 13, 2007; In Final Form: September 26, 2007

The intermediates ISO_3^- (m/z = 207) and $IS_2O_3^-$ (m/z = 239) generated in aqueous ($NaI/Na_2S_2O_3$) microdroplets traversing dilute O_3 gas plumes are detected via online electrospray mass spectrometry within ∼1 ms, and their stabilities gauged by collisionally induced dissociation. The simultaneous detection of anionic reactants and the $S_2O_6^{2-}$, HSO_4^-, IO_3^-, and I_3^- products as a function of experimental conditions provides evidence of genuinely interfacial reaction kinetics. Although O_3(aq) reacts about 3 times faster with I^- than with $S_2O_3^{2-}$ in bulk solution, only $S_2O_3^{2-}$ is significantly depleted in the interfacial layers of $[I^-]/[S_2O_3^{2-}]$ = 10 microdroplets below $[O_3(g)] \sim 50$ ppm.

Introduction

Atmospheric aerosols absorb and scatter solar radiation[1] and mediate important chemical processes.[2−5] Thus, for example, atmospheric SO_2 and NO_x can be oxidized in the gas phase, but acid rain results from their faster processing in aqueous aerosol droplets.[6−8] Although it has been speculated that they could display peculiar kinetic features, the analysis of gas−aerosol reactions remains wedded to data and concepts derived from studies performed in bulk solution.[9,10] If for no other reasons, the heretofore unknown chemical kinetics of bona fide interfacial reactions, and the reduced water activity prevalent in the aerial interfaces of atmospheric aerosol particles, should prevent the simple extrapolation of bulk data to the aerosol phase. The impasse is compounded by the technical difficulties associated with producing realistic aerosol particles and probing their chemical transformations while suspended in reactive atmospheres. Most studies, with a few exceptions,[11−13] have monitored the uptake of reactive gases by stationary trains of ∼10−100 μm droplets[14] that would have exceedingly large settling velocities (∼1 km day^{-1}), short residence times, and hence, negligible number densities in the atmosphere.[15]

Here we report novel experiments in which the chemical composition of aqueous submicron droplets undergoing chemical reaction with a reactive gas is directly monitored by electrospray mass spectrometry (ESMS) in ∼ 1 ms time frames. We chose to study the fast oxidations of I^-(aq) and $S_2O_3^{2-}$(aq) by O_3(g), which proceed at nearly diffusionally controlled rates in bulk solution,[16] in submicron droplets sprayed across dilute O_3/air gas plumes. We detect and quantify anion reactants and products, as well as the previously postulated short-lived reaction intermediates ISO_3^- and $IS_2O_3^-$. Our results show that this technique is capable of tracking chemical change in the condensed phase during fast aerosol−gas reactions. ESMS has been previously used for online monitoring of thermal, electrochemical, and photochemical reactions.[17−28]

Experimental Section

The experimental setup is shown in Figure 1A,B. Aqueous solutions (50 μL min^{-1}) were pumped into the reaction chamber through a grounded stainless steel needle injector (100 μM bore)[29]and pneumatically sprayed by means of nebulizer gas flowing coaxially. The difference between the velocities of the liquid jet (10.6 cm s^{-1}) and nebulizer gas (2.65 × 10^4 cm s^{-1}) is so large that the drag imposed on the liquid breaks it apart into micrometer size droplets. The terminal velocities of the microdroplets thus produced exceed ∼10^3 cm s^{-1},[30] which lead to transit times shorter than ∼1 ms across the ∼0.5 cm wide ozone plume. These droplets, which are produced by fragmentation of electrically neutral solutions from a grounded injector, are charged via statistical fluctuations that scale with (drop size)$^{-1/2}$.[31] The ensemble of spray droplets is on average neutral,

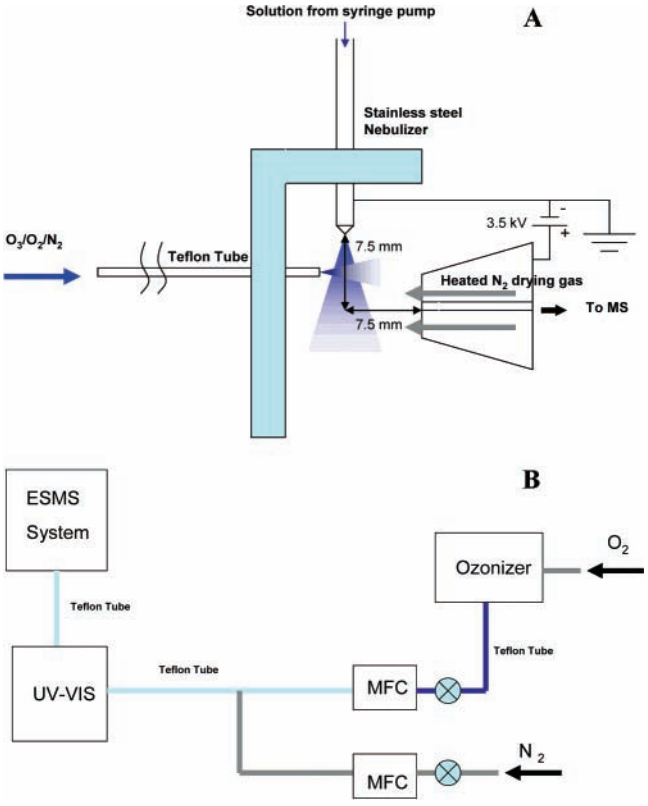

Figure 1. (A) Schematic diagram of electrospraying chamber and O_3-(g) injection system. (B) Overview of the experimental setup. MFC stands for mass flow controller.

* To whom corresponding should be addressed. Fax number: 626-395-2940. E-mail address: ajcoluss@caltech.edu.

10.1021/jp075505r CCC: $37.00
Published on Web 11/16/2007

TABLE 1: Kinetic and Equilibria Data in Aqueous Solution at 298 K

reaction number	reaction	rate or equilibrium constants (M, s units)	ref
R1	$I_2 + I^- \rightleftarrows I_3^-$	721 M^{-1}	56
R2	$I_2 + S_2O_3^{2-} \rightleftarrows I_2S_2O_3^{2-}$	7.8×10^9 M^{-1} s^{-1}	41
R-2		2.5×10^2 s^{-1}	
*R*3	$I_3^- + S_2O_3^{2-} \rightleftarrows I_2S_2O_3^{2-} + I^-$	4.2×10^8 M^{-1} s^{-1}	41
R-3		9.5×10^3 s^{-1}	
R4	$I_2S_2O_3^{2-} \rightleftarrows IS_2O_3^- + I^-$	0.245 M	41
R-4			
R5	$IS_2O_3^- + S_2O_3^{2-} \rightarrow I^- + S_4O_6^{2-}$	1.3×10^6 M^{-1} s^{-1}	41
R6	$I_3^- + 2S_2O_3^{2-} \rightarrow 3I^- + S_4O_6^{2-}$	N/A	
R7	$I_2 + HSO_3^- \rightarrow I_2SO_3^{2-} + H^+$	1.7×10^9 M^{-1} s^{-1}	41
R8	$I_3^- + HSO_3^- \rightarrow I^- + I_2SO_3^{2-} + H^+$	1.5×10^7 M^{-1} s^{-1}	44
R9	$I_2SO_3^{2-} \rightarrow ISO_3^- + I^-$	N/A	44
R10a	$S_2O_3^{2-} + O_3 \rightarrow S_2O_6^{2-}$	3.7×10^8 M^{-1} s^{-1}	38
R10b	$S_2O_3^{2-} + O_3 \rightarrow SO_4^{2-} + SO_2$		
R 11	$SO_2 + H_2O \rightleftarrows HSO_3^- + H^+$	1.3×10^{-2} M	62
R12	$I^- + O_3 + H^+ \rightarrow HOI + O_2$	1.2×10^9 M^{-1} s^{-1}	16
R13	$HOI + 2O_3 \rightarrow IO_3^- + 2O_2 + H^+$	3.6×10^4 M^{-1} s^{-1}	63
R14	$HOI + I^- + H^+ \rightarrow I_2 + H_2O$	4.4×10^{12} M^{-2} s^{-1}	64
R15	$HOI + S_2O_3^{2-} + H^+ \rightarrow IS_2O_3^- + H_2O$	N/A	
R16	$ISO_3^- + H_2O \rightarrow I^- + SO_4^{2-} + 2H^+$	298 s^{-1}	44

but individual droplets carry charges according to a Gaussian distribution, as expected for a random process. This largely unrecognized phenomenon is the basis, for example, of the classical oil drop experiment performed by Millikan to determine the magnitude of the elementary charge,[32] but it is not circumscribed to the laboratory. The finer seawater aerosol droplets, i.e., those that remain airborne long after being generated during bubble bursting, are negatively charged.[33] It should be emphasized that spontaneous, asymmetrical charge separation during pneumatic nebulization of liquids does not produce *highly charged* droplets and, therefore, is unrelated to electrospray ionization of droplets issuing from high-field nozzles.[34] Regardless of the charging mechanism, spray droplets eventually contract through solvent evaporation, a process regulated by ambient temperature and relative humidity, thereby increasing electrostatic repulsion among excess surface charges. Coulomb explosions ensue in which drops shed interfacial charge and mass into smaller droplets. These events, when replicated by progeny droplets both in the marine aerosol and in our spraying chamber, generate small particles that are multiplicatively enriched in tensioactive components. The final stage involves ion ejection from nanodroplets into the gas phase.[35] It is apparent that, by its very nature, this technique effectively samples the interfacial layers of the droplets.

Ozone was generated by flowing ultrapure O_2(g) (Air Liquide) through a commercial ozonizer (Ozone Solution), diluted 10-fold with ultrapure N_2(g), and quantified by UV absorption spectrophotometry (HP 8452) at 250 and 300 nm [absorption cross sections $\sigma(250\text{ nm}) = 1.1 \times 10^{-17}$, $\sigma(300\text{ nm}) = 3.9 \times 10^{-19}$ cm^2 $molecule^{-1}$ at 298 K][36] prior to entering the reaction chamber. Throughout, the reported [O_3(g)] values, which correspond to the concentrations actually sensed by the microdroplets in the reaction chamber, are estimated to be ~10 times smaller than the values determined from UV absorbances due to further dilution by the drying gas (Figure 1A). Gas flows were regulated by calibrated mass flow controllers (MKS). Typical instrumental parameters were as follows: drying gas temperature, 340 °C; nebulizer pressure, 28 psi; collector capillary voltage, +3.5 kV; fragmentor voltage, 22 V. Evidence that droplets are largely charged via statistical charge separation rather than by electrical field effects under present conditions is provided by Figure S3 (see Supporting Information) where we show that the kinetics of I^- oxidation by O_3(g) is unaffected by changing the capillary voltage from +1.5 to +3.5 kV relative to ground, i.e., to the needle injector. Solutions were prepared with MilliQ water that had been previously purged with ultrapure N_2(g) longer than 30 min. NaI (>99%), Na_2SO_3 (>98%), and $Na_2S_2O_3$ (>99.999%) were obtained from Sigma-Aldrich. Solutions pH was measured with a calibrated pH meter.

Results and Discussion

We have recently shown that I^- is rapidly oxidized to I_3^- and IO_3^- by O_3(g) at ppm levels in this experimental setup.[37] Thiosulfate is expected to react with O_3(g) at similar rates.[38] Because I_2/I_3^- also react rapidly with $S_2O_3^{2-}$, it should be possible to observe the transient intermediates $I_2S_2O_3^{2-}$ and $IS_2O_3^-$ proposed by Raschig a century ago to account for delayed formation tetrathionate (see also Table 1):[39−43]

$$I_2 + I^- \rightleftarrows I_3^- \qquad \text{(R1, R-1)}$$

$$I_2 + S_2O_3^{2-} \rightleftarrows I_2S_2O_3^{2-} \qquad \text{(R2, R-2)}$$

$$I_3^- + S_2O_3^{2-} \rightleftarrows I_2S_2O_3^{2-} + I^- \qquad \text{(R3, R-3)}$$

$$I_2S_2O_3^{2-} \rightleftarrows IS_2O_3^- + I^- \qquad \text{(R4, R-4)}$$

$$IS_2O_3^- + S_2O_3^{2-} \rightarrow I^- + S_4O_6^{2-} \qquad \text{(R5)}$$

A similar mechanism has been proposed for the $I_2/I_3^- + HSO_3^-/SO_3^{2-}$ reaction, which proceeds via the ISO_3^- intermediate.[44−47] The absorption spectra assigned by Packer and Anderson to $I_2S_2O_3^{2-}$ and $IS_2O_3^-$ intermediates in their pulse radiolysis experiments[48] are blue-shifted relative to those of I_3^- and I_2.

Identification of Anion Products and Intermediates. Figure 2 shows the mass spectra of aqueous $Na_2S_2O_3$ microdroplets in the absence and presence of O_3(g). Signals at $m/z = 112$, 135, and 293, which are ascribed to $S_2O_3^{\bullet-}$, $NaS_2O_3^-$, and $Na_3(S_2O_3)_2^-$, respectively, are observed in the absence of O_3(g). We detect the radical monoanion $S_2O_3^{\bullet-}$, rather than the closed-shell dianion $S_2O_3^{2-}$ ($m/z = 56$) in the ESMS of $Na_2S_2O_3$, in accord with previous reports.[49,50] Apparently, $S_2O_3^{2-}$(g) has negative electron affinity due to electrostatic repulsion between vicinal localized charges in $S{=}S(O)(O^-)_2$. The ready detection of $S_2O_8^{2-}$, in which charges are localized farther apart, supports this interpretation.[50] Field ejection of $S_2O_3^{2-}$ from charged nanodroplets[51] likely involves, therefore, concerted electron transfer to the solvent, i.e., $S_2O_3(H_2O)_n^{2-} \rightarrow S_2O_3^- + (H_2O)_n^-$. Thus, we consider $S_2O_3^{\bullet-}$ to be a valid marker of $S_2O_3^{2-}$ under

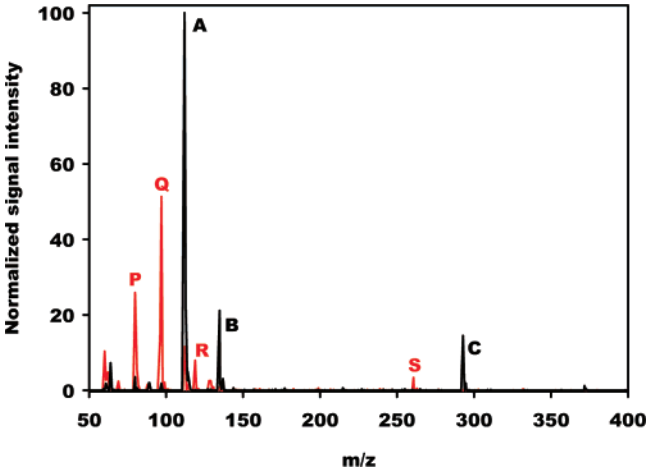

Figure 2. ESMS of (100 μM $Na_2S_2O_3$, pH 6.2) microdroplets in the presence of 640 ppm O_3(g) (red trace) and in its absence (black trace): A, m/z = 112 ($S_2O_3^-$); B, 135 ($NaS_2O_3^-$); C, 293 [$Na_3(S_2O_3)_2^-$]; P, 80 ($S_2O_6^{2-}$); Q, 97 (HSO_4^-); R, 119 ($NaSO_4^-$); S, 261 [$Na_3(SO_4)_2^-$].

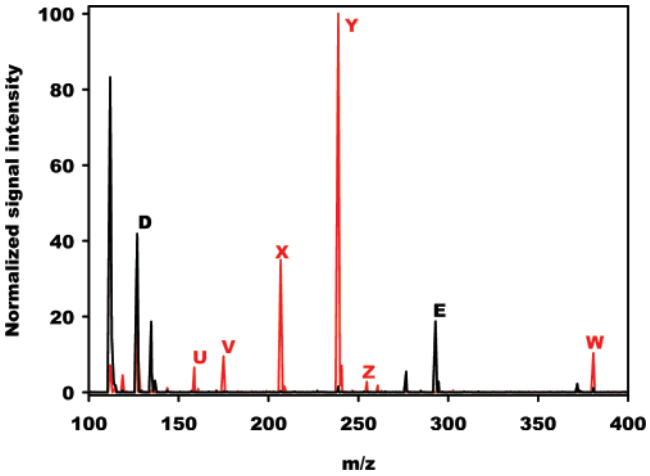

Figure 3. ESMS of (100 μM $Na_2S_2O_3$ + 100 μM NaI, pH 6.2) microdroplets in the presence of 760 ppm O_3(g) (red trace) and in its absence (black trace): D, m/z = 127 (I^-); E, 277 (NaI_2^-); U, 159 (IO_2^-), V, 175 (IO_3^-); W, 381 (I_3^-); X, 207 (ISO_3^-); Y, 239 ($IS_2O_3^-$); Z, 255 ($IS_2O_4^-$).

present conditions. In the presence of O_3(g), new signals at m/z = 80, 97, 119, and 261 appear, which correspond to $S_2O_6^{2-}$, HSO_4^-, $NaSO_4^-$, and $Na_3(SO_4)_2^-$, respectively.

Figure 3 shows a mass spectrum of NaI/$Na_2S_2O_3$ microdroplets reacting with O_3(g). The m/z = 175 and 381 signals correspond to IO_3^- and I_3^-, and the signals at m/z = 207 and 239 are assigned to the I−S species ISO_3^- and $IS_2O_3^-$, respectively. The m/z = 207 signal, accompanied by m/z = 97, 175, and 381 signals, is also produced in the reaction of NaI/Na_2SO_3 microdroplets with O_3(g). All product signals disappear at once upon discontinuing O_3(g) injection.

The identity of S-containing species was confirmed from the relative intensities of their M and M + 2 signals. Intensity ratios $M/(M+2)$ = 100/4.4, 100/8.8, and 100/17.6, are expected for natural ^{34}S-abundance compounds containing one, two, and four S-atoms, respectively. The measured (112)/(114) = 100/9.9, (207)/(209) = 100/5.6, and (239)/(241) = 100/10.3 ratios are therefore consistent with species containing two, one, and two S-atom(s), respectively, and exclude $S_4O_6^{2-}$, $I_2S_2O_6^{2-}$, or $I_2S_4O_6^{2-}$ species. We infer that the m/z = 207 and 239 signals correspond to ISO_3^- and $IS_2O_3^-$, respectively.

Mechanism of Reaction. Further information is gained by studying the dependence of signal intensities on [O_3(g)].

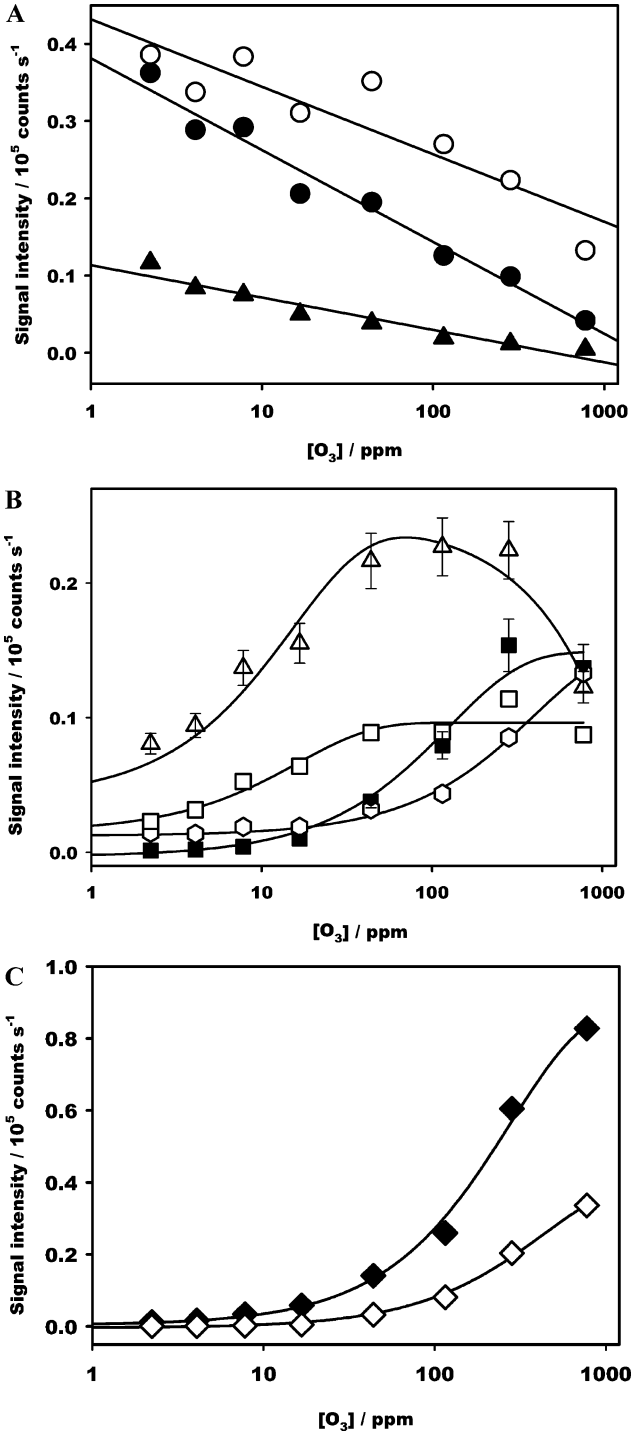

Figure 4. (A) ESMS signal intensities at m/z = 112 ($S_2O_3^-$, filled circle), 127 (I^-, open circle), and 135 ($NaS_2O_3^-$, filled triangle) vs [O_3(g)] in (100 μM $Na_2S_2O_3$ + 100 μM NaI, pH 6.2) microdroplets. (B) ESMS signal intensities at m/z = 80 ($S_2O_6^{2-}$, open triangle), 97 (HSO_4^-, open hexagon), 175 (IO_3^-, filled square), and 381 (I_3^-, open square) vs [O_3(g)] in (100 μM $Na_2S_2O_3$ + 100 μM NaI, pH 6.2) microdroplets. Error bars correspond to standard deviations of results of triplicate experiments. (C) ESMS signal intensities at m/z = 207 (ISO_3^-, open diamond) and 239 ($IS_2O_3^-$, filled diamond) vs [O_3(g)] in (100 μM $Na_2S_2O_3$ + 100 μM NaI, pH 6.2) microdroplets.

Reactant anion signal intensities at m/z = 112 ($S_2O_3^-$), 127 (I^-), and 135 ($NaS_2O_3^-$) decline with increasing [O_3(g)], as shown in Figure 4A. Product and intermediate anion signal intensities at m/z = 80 ($S_2O_6^{2-}$), 97 (HSO_4^-), 119 ($NaSO_4^-$), 175 (IO_3^-), 381 (I_3^-), 207 (ISO_3^-), and 239 ($IS_2O_3^-$) are all enhanced upon

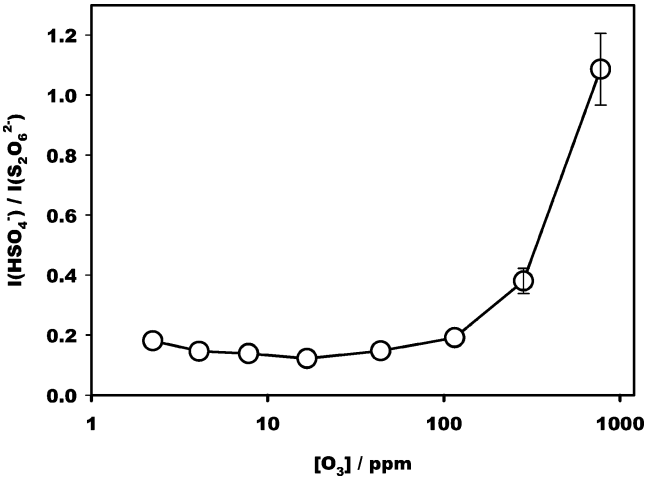

Figure 5. Ratio of signal intensities at $m/z = 97$ and 80: $I(HSO_4^-)/I(S_2O_6^{2-})$ vs $[O_3(g)]$ in (100 μM $Na_2S_2O_3$ + 100 μM NaI, pH 6.2) microdroplets. Error bars correspond to standard deviations of results of triplicate experiments and are smaller than symbol size below 100 ppm $O_3(g)$.

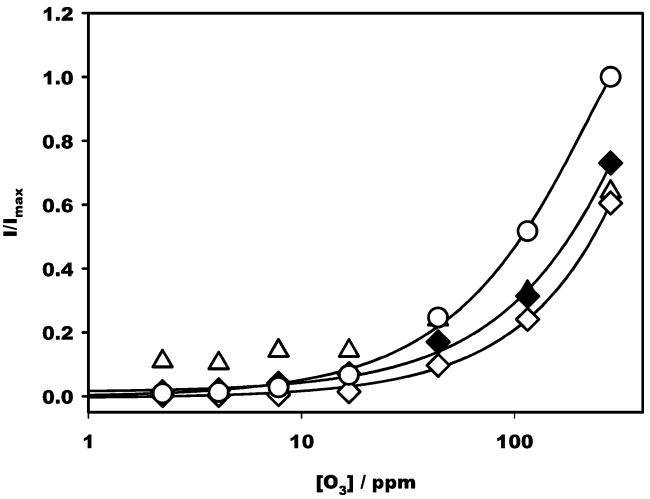

Figure 6. Normalized ESMS signal intensities I at $m/z = 97$ (HSO_4^-, open triangle), 175 (IO_3^-, open circle), 207 (ISO_3^-, open diamond), and 239 ($IS_2O_3^-$, filled diamond) vs $[O_3(g)]$ in (100 μM $Na_2S_2O_3$ + 100 μM NaI, pH 6.2) microdroplets.

increasing $[O_3(g)]$, as shown in Figure 4B,C. Note the upward inflections observed at ~50 ppm $O_3(g)$ in Figure 4B,C.

Figure 5 shows a plot of the $[HSO_4^-]/[S_2O_6^{2-}]$ ratio as function of $[O_3(g)]$. A nonvanishing value below ~50 ppm $O_3(g)$ is a direct indication that $S_2O_6^{2-}$ and HSO_4^- are primary species produced in competing pathways, reactions 10a and 10b in Table 1.[52] The marked increase of this ratio at higher $[O_3(g)]$ shows that further HSO_4^- is produced, in the oxidation of reactive byproducts. This interpretation is confirmed by the inertness of 0.1 mM $S_2O_6^{2-}$ toward O_3, together with the lack of HSO_4^- ($m/z = 97$) production below 420 ppm $O_3(g)$ (see Supporting Information). A 0.25 mM $S_4O_6^{2-}$ solution, prepared by titration of 0.5 mM $S_2O_3^{2-}$ with I_3^-:[53]

$$I_3^- + 2S_2O_3^{2-} \rightarrow 3I^- + S_4O_6^{2-} \qquad \text{(R6)}$$

and subsequently sprayed in the reaction chamber, is inert toward $O_3(g)$. The $m/z = 112$ ($S_4O_6^{2-}$) and 97 (HSO_4^-) signal intensities remain constant below 520 ppm $O_3(g)$.

Figure 6 shows how ISO_3^-, $IS_2O_3^-$, HSO_4^-, and IO_3^- signal intensities vary with $[O_3(g)]$, indicating that HSO_4^-, IO_3^-, ISO_3^-, and $IS_2O_3^-$ are later generation species whose rates of formation have a stronger dependence on $[O_3(g)]$ than those of $S_2O_6^{2-}$ and I_3^-.

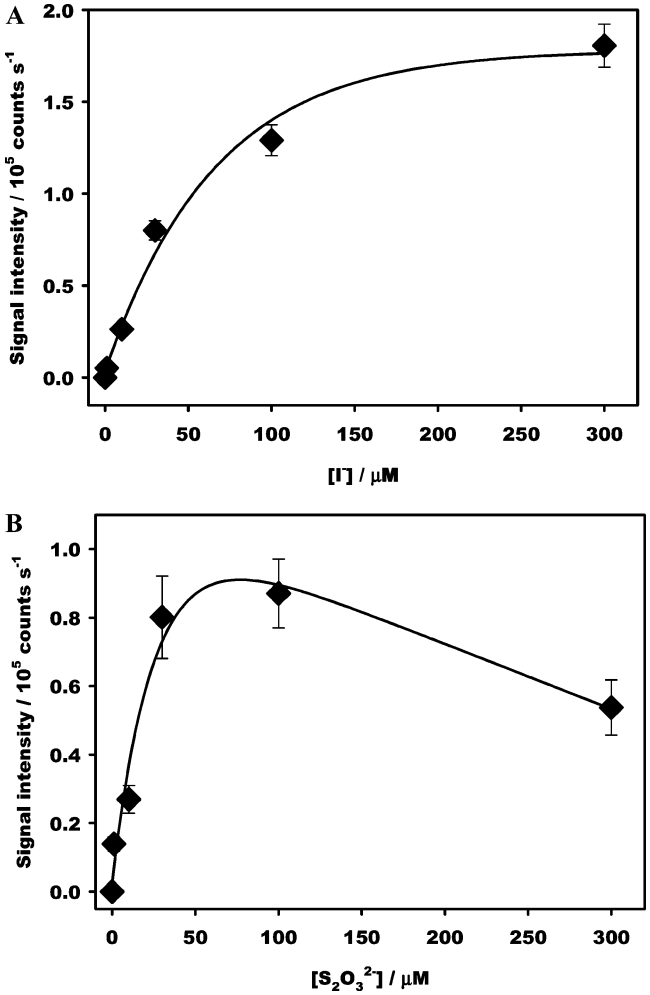

Figure 7. (A) $IS_2O_3^-$ signal intensities vs $[NaI]_0$ in (30 μM $Na_2S_2O_3$ + NaI, pH 6.2) microdroplets at $[O_3(g)] = 300$ ppm. (B) $IS_2O_3^-$ signal intensities vs $[Na_2S_2O_3]_0$ in ($Na_2S_2O_3$ + 30 μM NaI, pH 6.2) microdroplets at $[O_3(g)] = 350$ ppm.

We recently found that in this setup the oxidation of I^- by $O_3(g)$ yields iodate, IO_3^-, and triiodide, I_3^- (reactions R12−R14).[29] I_3^- is in equilibrium with I^- and I_2[54−57] (reaction R1). I_3^- and/or I_2 can then react with HSO_3^- or $S_2O_3^{2-}$ according to reactions R2 and R3 and R7 and R8.[28,32] The fact that we do not observe $I_2SO_3^{2-}$ ($m/z = 167$) or $I_2S_2O_3^{2-}$($m/z = 183$) in NaI/Na_2SO_3 or $NaI/Na_2S_2O_3$ droplets in contact with $O_3(g)$ implies that their decomposition lifetimes are much shorter than ~1 ms under the present conditions (reactions R-4 and R9), in accord with Margerum et al.[32] $I_2S_2O_3^{2-}$ is thermodynamically stable ($k_2/k_{-2} = K_2 = 3.2 \times 10^7$ M^{-1}), but kinetically reactive ($k_4/k_{-4} = K_4 = 0.245$ M). The dissociation equilibrium constant of $I_2S_2O_3^{2-}$, $K_4 = 0.245$ M, is ~100 times larger than that of I_3^-, $k_{-1}/k_1 = 1.39 \times 10^{-3}$ M.[58] Our results do not exclude, however, the participation of hypoiodous acid, HOI, which is considered to be more reactive than I_2 or I_3^- as oxidant:

$$HOI + S_2O_3^{2-} + H^+ \rightarrow IS_2O_3^- + H_2O \qquad \text{(R15)}$$

The dependence of $IS_2O_3^-$ ($m/z = 239$) signal intensity in 30 μM $Na_2S_2O_3$ droplets as a function of [NaI] in the range of 1−300 μM, at constant $[O_3(g)] = 300$ ppm, is shown in Figure 7A. The observed exponential growth to a maximum is

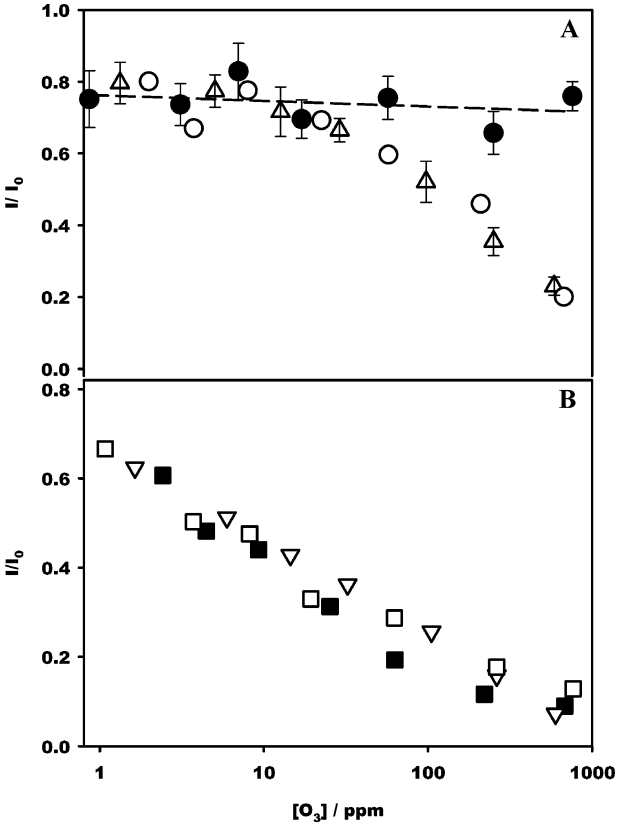

Figure 8. (A) Normalized ESMS signal intensities I at $m/z = 127$ (I^-) in ($[NaI]_0 = [Na_2S_2O_3]_0 = 30\ \mu M$) (open triangle), ($[NaI]_0 = 300$, $[Na_2S_2O_3]_0 = 30\ \mu M$) (open circle), and ($[NaI]_0 = 30$, $[Na_2S_2O_3]_0 = 300\ \mu M$) (closed circle) microdroplets vs [O_3(g)]. (B) Normalized ESMS signal intensities I at $m/z = 112$ ($S_2O_3^-$) in ($[NaI]_0 = [Na_2S_2O_3]_0 = 30\ \mu M$) (open triangle), ($[NaI]_0 = 300$, $[Na_2S_2O_3]_0 = 30\ \mu M$) (open square), and ($[NaI]_0 = 30$, $[Na_2S_2O_3]_0 = 300\ \mu M$) (filled square) microdroplets vs [O_3(g)].

qualitatively consistent with the proposed mechanism of formation. Figure 7B shows the dependence of $IS_2O_3^-$ ($m/z = 239$) signal intensity in 30 μM NaI droplets as a function of $[Na_2S_2O_3]$ in the range 1−300 μM, at constant [O_3(g)] = 350 ppm. In contrast with the behavior observed in Figure 7A, $IS_2O_3^-$ peaks at $[Na_2S_2O_3] \sim 100\ \mu M$. This response implies that $S_2O_3^{2-}$ participates in both the formation and destruction of $IS_2O_3^-$ and is consistent with the increasing role of reaction 5 at higher $[Na_2S_2O_3]$:[32]

$$IS_2O_3^- + S_2O_3^{2-} \rightarrow I^- + S_4O_6^{2-} \qquad \text{(R5)}$$

From the reported value of $k_5 = 1.29 \times 10^6\ M^{-1}\ s^{-1}$, we estimate that the half-life of $IS_2O_3^-$ in reaction 5 is ~5 ms at $[Na_2S_2O_3] \sim 100\ \mu M$, which provides a direct measure of our temporal window. The rapid hydrolysis of ISO_3^- (reaction R16) regenerates I^-,[44] and may be responsible for the results shown in Figure 8 A (see below).

Interfacial Reaction Kinetics. Figure 8 shows the dependence of [I^-] and [$S_2O_3^{2-}$] versus [O_3(g)] in three different solutions: $[NaI]_0 = [Na_2S_2O_3]_0 = 30\ \mu M$ (A), $[NaI]_0 = 10 \times [Na_2S_2O_3]_0 = 300\ \mu M$ (B), and $[Na_2S_2O_3]_0 = 10 \times [NaI]_0 = 300\ \mu M$ (C). $S_2O_3^{2-}$ undergoes significant oxidation in all cases over the entire [O_3(g)] range covered in these experiments. In contrast, I^- oxidation sets off above [O_3(g)] ~50 ppm in the A and B mixtures and is fully inhibited in C. Because O_3(aq) reacts ~3 times faster with I^- than with $S_2O_3^{2-}$ in the bulk (see Table 1) these observations imply that the interfacial layers of the

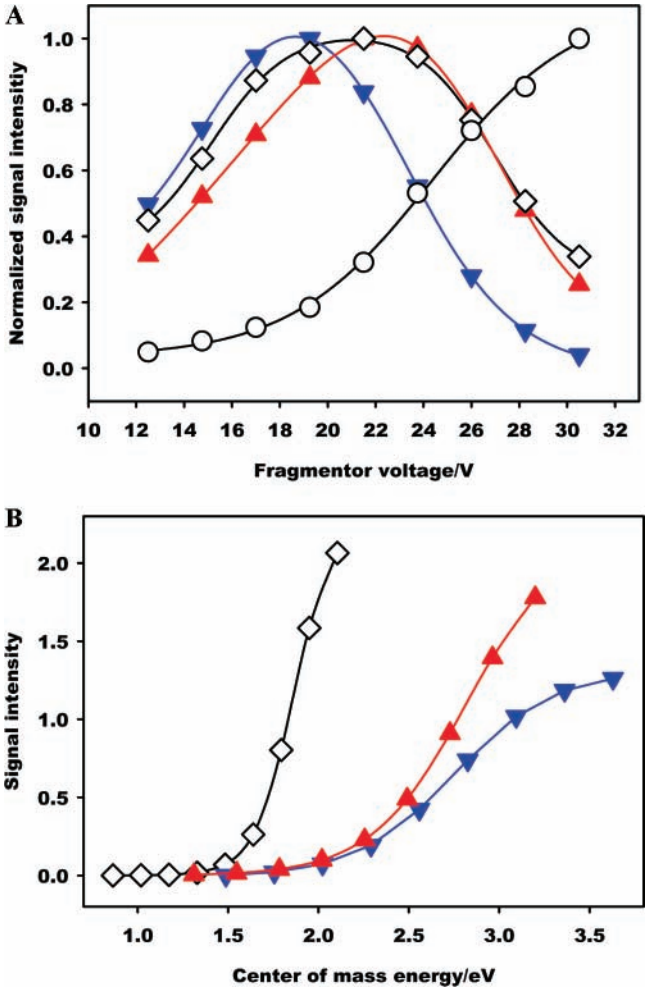

Figure 9. (A) Fragmentor voltage effects on ESMS normalized signal intensities in ($[NaI]_0 = [Na_2S_2O_3]_0 = 100\ \mu M$) microdroplets at [$O_3$(g)] = 410 ppm: I^-, open circle; ISO_3^-, downward filled triangle; $IS_2O_3^-$, upward filled triangle; I_3^-, open diamond. (B) Deconvoluted ESMS signal intensities vs center of mass energy: I_3^-, open diamond; ISO_3^-, downward filled triangle; $IS_2O_3^-$, upward filled triangle. See text for details.

droplets are predominantly populated by $S_2O_3^{2-}$ and/or that reactivities at the air−water interface are significantly different than in the bulk. Considering that the ratio of signal intensities: $I(S_2O_3^{\bullet-})/I(I^-) = 1.2 \pm 0.1$, in equimolar $Na_2S_2O_3$/NaI solutions is a direct measure of the relative affinities of $S_2O_3^{2-}$ and I^- for the interfacial layers of microdroplets, we conclude that their relative reactivities toward O_3(g) are indeed reversed relative to the bulk. Note that a decrease of I^- at [O_3(g)] ≥ 50 ppm in Figure 8A coincides with the onset of the $IS_2O_3^-$ and ISO_3^- in Figure 4C, supporting the proposed involvement of the products of I^- oxidation in their mechanism of formation.

Stability of Intermediates. We probed the thermal stability of ISO_3^-, $IS_2O_3^-$, and I_3^- in the gas phase via collisionally induced dissociation experiments, in which the variation of ion signal intensities were recorded as a function of fragmentor voltage (FV). FV is the electrical potential difference between the capillary exit and the first skimmer, a region where ions are accelerated up to excess kinetic energies given by KE = FE × $q_i = {}^1/_2 m_i v_i^2$; q_i is the charge, m_i is the mass, and v_i is the excess velocity of ion i, respectively. Molecular ions convert their excess KE into internal (vibrational/rotational) excitation during impact with (N_2) bath gas molecules prior to undergoing collisionally induced dissociation.[59] Figure 9A shows the dependence of $m/z = 127$ (I^-), 207 (ISO_3^-), 239 ($IS_2O_3^-$), and

381 (I_3^-) signal intensities on FV. FV effects on other species are provided as Supporting Information. The monotonous increase of the I^- signal reveals that ion collection efficiencies generally increase with FV. The maxima observed in the case of ISO_3^-, $IS_2O_3^-$, and I_3^- indicates, therefore, the onset of fragmentation. Curve deconvolution into two sigmoids, followed by the conversion of laboratory (KE) to center-of-mass (CEM) kinetic energies [CEM = $m/(m + M)$ KE, where $m = 28$ is the molecular mass of the N_2 collider gas and $M = 207$, 239, or 381, the molecular masses of the various anions] leads to the fragmentation curves shown in Figure 9B. Threshold CEM energies are consistent with the reported values for BDE($I^- - I_2$) = 1.31 eV,[60] and BDE($I^- - SO_3$) = 1.67 eV.[61] The fact that $IS_2O_3^-$ and ISO_3^- have similar stabilities in the gas phase suggests the presence of weak I−S bonds in both species.[32]

Acknowledgment. This work was financially supported by the National Science Foundation grant ATM-0534990. We thank Nathan F. Dalleska for valuable advice on ESMS, and Mike Vondrus for assistance in setting up the ozone injector. S.E. is grateful to Prof. M. Kawasaki (Kyoto University), Prof. Y. Matsumi (Nagoya University), and the JSPS Research Fellowship for Young Scientists.

Supporting Information Available: Plots of MS signal intensities, fragmentor voltage effects on signal intensities, voltage effects on [$I^- + O_3$(g)] kinetics. This material is available free of charge via the Internet at http://pubs.acs.org.

References and Notes

(1) Satheesh, S. K.; Moorthy, K. K. *Atmos. Environ*. **2005**, *39*, 2089.
(2) Herrmann, H. *Chem. Rev.* **2003**, *103*, 4691.
(3) Reid, J. P.; Sayer, R. M. *Chem. Soc. Rev.* **2003**, *32*, 70.
(4) Nissenson, P.; Knox, C. J. H.; Finlayson-Pitts, B. J.; Phillips, L. F.; Dabdub, D. *Phys. Chem Chem. Phys.* **2006**, *8*, 4700.
(5) Pilinis, C.; Pandis, S. N.; Seinfeld, J. H. *J. Geophys. Res.* **1995**, *100*, 18739.
(6) Hoffmann, M. R.; Edwards, J. *J. Phys. Chem.* **1975**, *79*,2096.
(7) Mcardle, J. V.; Hoffmann, M. R. *J. Phys. Chem*. **1983**, *87*, 5425.
(8) Hoffmann, M. R. *Atmos. Environ*. **1986**, *20*, 1145.
(9) Hunt, S. W.; Roeselova, M.; Wang, W.; Wingen, L. M.; Knipping, E. M.;Tobias, D. J.; Dabdub, D.; Finlayson-Pitts, B. J. *J. Phys. Chem. A* **2004**, *102*, 11559.
(10) Hu, J. H.; Shi, Q.; Davidovitz, P.; Worsnop, D. R.; Zahniser, M. S.; Kolb, C. E. *J. Phys. Chem.* **1995**, *99*, 8768.
(11) Schütze, M.; Herrmann, H. *Phys. Chem. Chem. Phys.*. **2006**, *4*, 60.
(12) Tolocka, M. P.; Saul, T. D.; Johnston, M. V. *J. Phys. Chem. A* **2004**, *108*, 2659.
(13) González-Labrada, E.; Schmidt, R.; DeWolf, E. *Chem. Commun*. **2006**, *23*, 2471.
(14) Davidovits, P.; Kolb, C. E.; Williams, L. R.: Jayne, J. T.; Worsnop, D. R. *Chem. Rev*. **2006**, *106*, 1323.
(15) Finlayson-Pitts, B. J.; Pitts, J. N. *Chemistry of the upper and lower atmosphere*; Academic Press: San Diego, CA, 2000; p 364.
(16) Liu, Q.; Schurter, L. M.; Muller, C. E.; Aloisio, S.; Francisco, J. D.; Margerum, D. W. *Inorg. Chem.* **2001**, *40*, 4436.
(17) Espenson, H. E.; Tan, H.; Mollah, S.; Houk, R. S.; Eager, M. D. *Inorg. Chem.* **1998**, *37*, 4621.
(18) Bakhtiar, R.; Hop, C. E. C. A. *J. Phys. Org. Chem*. **1999**, *12*, 511.
(19) (a) Arakawa R.; Liu, J.; Mizuno, K.; Inoue, H.; Doe H.; Matsuo, T. *Int. J. Mass Spectrom*. **1997**, *160*, 371. (b) Arakawa, R.; Jian, L.; Yoshimura, A.; Nozaki, K.; Ohno, T.; Doe, H.; Matsuo, C.; Arakawa, R.; Tachiyashiki, S.; Matsuo, T. *Anal. Chem*. **1995**, *67*, 4133. (c) Arakawa, R.; Mimura, S.; Mastsubayashi, G.; Matsuo, T. *Inorg. Chem*. **1996**, *35*, 5725. (d) Arakawa, R.; Matsuda, F.; Mastsubayashi, G. *Am. Soc. Mass Spectrom*. **1997**, *8*, 713.
(20) Aliprantis, A. O.; Canary, J. W. *J. Am. Chem. Soc*. **1994**, *116*, 6985.
(21) Brum, J.; Dell'Orco, P.; Lapka, S.; Muske, K.; Sisko, J. *Rapid Commun. Mass Spectrom*. **2001**, *15*, 1548.
(22) Zechel, D. L.; Konermann, L.; Withers, S. G.; Douglas, D. J. *Biochemistry* **1998**, *37*, 7664.
(23) Xu, X.; Lu, W.; Cole, R. B. *Anal. Chem*. **1996**, *68*, 4244.
(24) Brum, J.; Dell'Orco, P. *Rapid Commun. Mass Spectrom*. **1998**, *12*, 741.
(25) Volmer, D. A. *J. Chromatogr. A* **1998**, *794*, 129.
(26) Santos, L. S.; Knaack, L.; Metzger, J. O. *Int. J. Mass. Spectrosc.* **2005**, *246*, 84.
(27) Ding, W.; Johnson, K. A.; Kutal, C.; Amster, I. J. *Anal. Chem.* **2003**, *75*, 4624.
(28) Thomas, M. C.; Mitchell, T. W.; Blanksby, S. J. *J. Am. Chem. Soc*. **2005**, *128*, 58.
(29) Cheng. J.; Vecitis, C. D.; Hoffmann, M. R.; Colussi, A. J. *J. Phys. Chem. B.* **2006**, *110*, 25598.
(30) Kahen, K.; Jorabchi, K.; Gray, C.; Montaser, A. *Anal. Chem*. **2004**, *76*, 7194.
(31) Dodd, E. E. *J. Appl. Phys.* **1953**, *24*, 73.
(32) Millikan, R. A. *Science* **1910**, *32*, 436.
(33) Reiter, R. *J. Geophys. Res.* **1994**, *99*, 10807.
(34) Fenn, J. B. *J. Am. Soc. Mass Spectrom.* **1993**, *4*, 524.
(35) Kebarle, P. *J. Mass Spectrom.* **2000**, *35*, 804.
(36) Sander, S. P.; et al. Chemical Kinetics and Photochemical Data for Use in Stratospheric Modeling; Evaluation 15; Jet Propulsion Laboratory: Pasadena, CA, 2006.
(37) Enami, S.; Vecitis, C. D.; Cheng. J.; Hoffmann, M. R.; Colussi, A. J. *J. Phys. Chem. A* **2007**, *111*, 8749.
(38) Muller, B.; Heal, M. R. *Phys. Chem. Chem. Phys.* **2002**, *4*, 3365.
(39) Raschig, F. *Chem. Ztg.* **1908**, *32*, 1203.
(40) Raschig, F. *Ber. Dtsch. Chem. Ges.* **1915**, *48*, 2088.
(41) Scheper, W. M.; Margerum, D. W. *Inorg. Chem*. **1992**, *31*, 5466.
(42) Dodd, G.; Griffith, R. O. *Trans. Faraday. Soc.* **1949**, *45*, 546.
(43) Awtrey, A.; Connick, R. E. *J. Am. Chem. Soc*. **1951**, *73*, 1341.
(44) Yiin B. S.; Margerum, D. W. *Inorg. Chem.* **1990**, *29*, 1559.
(45) Landolt, H. *Ber. Dtsch. Chem. Ges.* **1886**, *19*, 1317.
(46) Bunau, G. V.; Eigen, M. *Z. Phys. Chem.* (*Frankfurt*) **1962**, *32*, 27.
(47) Inoue, H.; Sudo, Y. *Kogyo Kagaku Zasshi* **1967**, *70*, 123.
(48) Packer, J. E.; Anderson, R. F. *Aust. J. Chem*. **1997**, *50*, 435.
(49) Stewart, I. I.; Barnett, D. A.; Horlick, G. *J. Anal. Atom. Spectrosc.* **1996**, *11*, 877.
(50) Agnes, G. R.; Stewart, I. I.; Horlick, G. *Appl. Spectrosc.* **1994**, *48*, 1347.
(51) Kebarle, P. *J. Mass Spectrom.* **2000**, *35*, 804.
(52) *Gmelins Handbuch der anorganischen Chemie*, *Schwefel*; Verlag: Weinheim, 1960; Teil B, Lieferung 2, p 896 (see also references therein).
(53) Harris, W. E.; Daniel, C. Q*uantitative Chemical Analysis*, 3rd ed.; Freeman: New York, 1991.
(54) Myers, O. E. *J. Chem. Phys*. **1958**, *28*, 1027.
(55) Ramette, R. W.; Sandford, R. W., Jr. *J. Am. Chem. Soc.* **1965**, *87*, 5001.
(56) McIndoe, J. S.; Tuck, D. G. *Dalton Trans*. **2003**, *2*, 244.
(57) Troy, R. C.; Kelly, M. D.; Nagy, J. C.; Margerum, D. W. *Inorg. Chem.* **1991**, *30*, 4838.
(58) Ramette, R. W.; Sandford, R. W. *J. Am. Chem. Soc*. **1965**, *87*, 5001.
(59) Schneider, B. B.; Chen, D. Y. *Anal. Chem.* **2000**, *72*, 791.
(60) Nizzi, K. E.; Pommerening, C. A.; Sunderlin, L. S. *J. Phys. Chem. A* **1998**, *102*, 7674.
(61) Hao, C.; Gilbert, T. M.; Sunderlin, L. S. *Can. J. Chem.* **2005**, *83*, 2013
(62) Sillén, G. H.; Martell, A. E. *Stability Constants of Metal-Ion Complexes*; Special Publication 17; Chemical Society: London, 1964.
(63) Bichsel, Y.; von Gunten, U. *Environ. Sci. Technol*. **1999**, *33*, 4040.
(64) Eigen, M.; Kustin, K. *J. Am. Chem. Soc.* **1962**, *84*, 1355.